HYPERSONIC TARGET DETECTION USING EOIR-EMULATED SYNTHETIC DATA: A CASE STUDY OF X-43A

Slobodan Pajić[1]*,
[0000-0002-6883-8550]

Gerrit Viljoen[1],
[0009-0007-3825-8444]

Marko Tanasković[2]
[0000-0003-3592-0598]

[1]Halcon, EDGE group,
Abu Dhabi, UAE

[2]Singidunum University,
Belgrade, Serbia

Abstract:

Detecting hypersonic vehicles is challenging due to their high flight velocity, unpredictable flight paths, and distinct thermal signatures. This study used the ANSYS Systems Tool Kit (STK) to generate high-fidelity synthetic datasets. These datasets were designed to simulate Electro-Optic Infrared (EOIR) scenarios tailored specifically for hypersonic targets. Inspired by the X-43A hypersonic flight tests, we created a simplified environment without terrain modeling to balance computational efficiency and physics-based simulation. Our approach tackles the critical lack of real-world data by offering a scalable and realistic foundation for advancing Automatic Target Recognition (ATR) systems. Our simulations demonstrated that a Modified HALO-II sensor achieved an 18% improvement in detection rates compared to the standard HALO-II sensor, even under challenging thermal conditions. We explain the experimental setup and ATR dataset generation. Future work will focus on integrating synthetic with experimental datasets to help AI-driven detection systems address the evolving challenges of hypersonic threats.

Keywords:

Synthetic Image Generation, EOIR, Hypersonic Targets, ANSYS STK, ATR.

INTRODUCTION

1.1. BACKGROUND ON THE X-43A PROGRAM

NASA's X-43A program was part of the broader Hyper-X initiative, which marked a substantial breakthrough in hypersonic propulsion technology from multiple perspectives. This experimental vehicle successfully showed that a scramjet engine (short for supersonic combustion ramjet) could be combined with an airframe to achieve stable hypersonic flight. The program was launched in 1995-1996 to validate scramjet operability and generate data for designing future airbreathing hypersonic cruise platforms. The X-43A's successful flights in 2004 at Mach 7 and Mach 10 marked a significant advancement in hypersonic propulsion for US domestic capabilities [1], [2], [3].

The scramjet engine used gaseous hydrogen as fuel, with silane as its igniter. Its design was integrated seamlessly with the airframe, using the vehicle's forebody and afterbody as compression and expansion surfaces to maintain efficient airflow through the engine at hypersonic speeds.

Correspondence:
Slobodan Pajić

e-mail:
pajic428@gmail.com

DOI: 10.15308/Sinteza-2025-251-258

Thermal protection was a crucial aspect of the design. Reinforced carbon-carbon was used for leading edges, and aluminium-enhanced thermal barrier tiles were used to shield the vehicle from extreme aerodynamic heating. The Mach 10 configuration incorporated enhanced thermal protections compared to the Mach 7 design, reflecting the higher thermal loads encountered at such speeds. The structure was composed of steel, titanium, and tungsten, materials chosen for their stiffness and thermal properties [3], [4]. The X-43A program's detailed aerodynamic and thermal performance datasets provided a foundational framework for modeling realistic EOIR target scenarios in this study.

The flight tests conducted as part of the Hyper-X program were very valuable. After a failed first flight in 2001 due to a booster malfunction, two successful flights in 2004 validated the scramjet engine's performance. On March 27, 2004, the X-43A achieved Mach 6.83; on November 16, 2004, it reached Mach 9.68, setting records for the fastest speeds ever achieved by an airbreathing vehicle. These tests confirmed that airframe-integrated scramjets could operate autonomously. These experiments produced data critical for validating computational models, aerodynamics, propulsion systems, and thermal management material technologies [2]- [4].

One of the significant challenges addressed during the program was achieving the necessary structural stiffness for the vehicle. Engineers relied heavily on finite element analysis to design a robust structure since intense bending moments were analyzed during flight. Vehicle weight was problematic since extensive usage of steel and aluminum was used to help with the structure rigidity. Despite these challenges, the X-43A transitioned smoothly between subsonic and supersonic combustion modes—a crucial feature of dual-mode scramjet engine design. This success was thanks to cutting-edge computational fluid dynamics (CFD) simulations and thorough wind tunnel testing [4].

The program also produced significant advancements in instrumentation and data acquisition. The X-43A was equipped with more than 500 sensors, including pressure taps and thermocouples, to gather precise data on the vehicle's aerodynamic pressure field, thermal characteristics, and structural performance. This array of instruments was used to deliver real-time data with telemetry equipment during the flights, allowing engineers to thoroughly analyze the vehicle's behavior and performance while flying at hypersonic speeds [3], [4].

The influence of the X-43A program goes far beyond its initial achievements. Proving that scramjet-powered hypersonic flight is possible paved the way for future innovations, such as reusable launch vehicles (RLVs) and hypersonic cruise missiles. Moreover, the data and insights gained have informed ongoing research into combined-cycle propulsion systems, such as Turbine-Based Combined Cycle (TBCC) and Rocket-Based Combined Cycle (RBCC) architectures [2]- [4].

1.2. CHALLENGES IN HYPERSONIC SCENARIO MODELLING

Hypersonic vehicles are complicated to detect and track because of their high speeds, unpredictable trajectories, and the intense heat generated by aerodynamic forces. Simulating these conditions using physics-based methods is particularly challenging for several reasons. Using synthetic data is a helpful way to recreate the extreme speeds and intense heat that hypersonic vehicles experience. It also reduces the need for expensive and potentially risky real-world data collection. The availability of real-world datasets for hypersonic scenarios is limited, mainly because of operational difficulties and strict confidentiality rules. Synthetic image generation allows the creation of datasets designed explicitly for automatic target recognition (ATR). Electro-optic infrared (EOIR) sensor models are key to making this process work effectively. Recreating critical elements of the X-43A flight test in synthetic environments establishes a robust foundation for further research or automatic target recognition (ATR) in the multispectral domain.

1.3. RESEARCH APPROACH AND OBJECTIVES

This study employs ANSYS STK tools to generate EOIR-emulated synthetic datasets, replicating the X-43A flight test scenario and expanding it with EOIR-rendered images. The approach minimizes computational complexity by simplifying the problem to flying objects without terrain while preserving operational relevance. The findings will demonstrate the potential of synthetic data in advancing hypersonic research.

2. RELATED WORK AND LITERATURE REVIEW

Synthetic data generation has revolutionized fields dependent on large-scale datasets by providing automated annotations, eliminating the time-consuming and costly manual labeling process. Despite its advantages, challenges such as domain adaptation and achieving realism persist when applying synthetic data to real-world scenarios [5], [6]. Two dominant approaches have emerged: domain randomization and photorealistic rendering. Domain randomization introduces diverse variations, such as lighting and object poses, to train robust neural networks [7]. Realistic rendering emphasizes visually accurate scenes with diverse environmental conditions like seasons and lighting [8], [9].

In defense applications, synthetic data has been instrumental in object detection and segmentation, with tools like DIRSIG modeling complex environments, including atmospheric and thermal conditions [6], [10]. Combining synthetic and real-world datasets, hybrid methods address the domain gap and enhance performance [6], [11]. These methodologies are well-suited for hypersonic scenarios, where challenges like high-speed targets and dynamic thermal signatures demand advanced synthetic datasets. Supported by tools such as STK EOIR, this study fills the gap by adapting synthetic data techniques to hypersonic detection [6], [10].

3. METHODOLOGY

The ANSYS STK EOIR module was the basis of this research. This tool provided high-fidelity radiometric sensor modeling, atmospheric effects simulation, and synthetic scenario scene generation. Using its capabilities, we simulated realistic hypersonic flight conditions and generated synthetic imagery to support developing and evaluating detection and tracking algorithms.

3.1. EXPERIMENTAL SETUP

Researchers developed the setup for studying the X-43A's flight, making sure it could accurately capture data during the vehicle's unpowered trajectory. Thanks to this detailed preparation, they were able to gather valuable insights into the vehicle's aerodynamic, thermal, and structural performance. As a result, researchers could thoroughly analyze and validate how the X-43A behaved while flying at hypersonic speeds [3], [4]. The mission employed a B-52 aircraft as the launch platform, following a pre-defined trajectory to achieve the specific altitude, velocity, and trajectory angles necessary to deploy the X-43A and its booster. The booster rocket carrying the X-43A was launched at the designated release point. Following the booster burn phase, a controlled separation was executed. Subsequently, the sustainer scramjet motor was activated, as illustrated in Figure 1 (a). Upon completion of the sustainer burn phase, depicted in Figure 1 (b), data about the unpowered flight phase was recorded precisely.

3.2. SCENARIO SETUP

We adopted a step-by-step approach to simulating the operational environment of X-43A hypersonic vehicle. The hypersonic vehicle was modeled with precise geometrical details, including surface materials characterized by their optical and thermal properties. The vehicle's path mimicked real-world flight dynamics, including fast acceleration, high-speed cruising, and gradual deceleration.

The simulation included atmospheric conditions that changed to match different operating scenarios, such as variations in temperature, pressure, humidity, and solar radiation. MODTRAN-based atmospheric models incorporated environmental effects such as transmission losses, scatter, and thermal path radiance. Scenarios included clear skies and degraded visual environments like

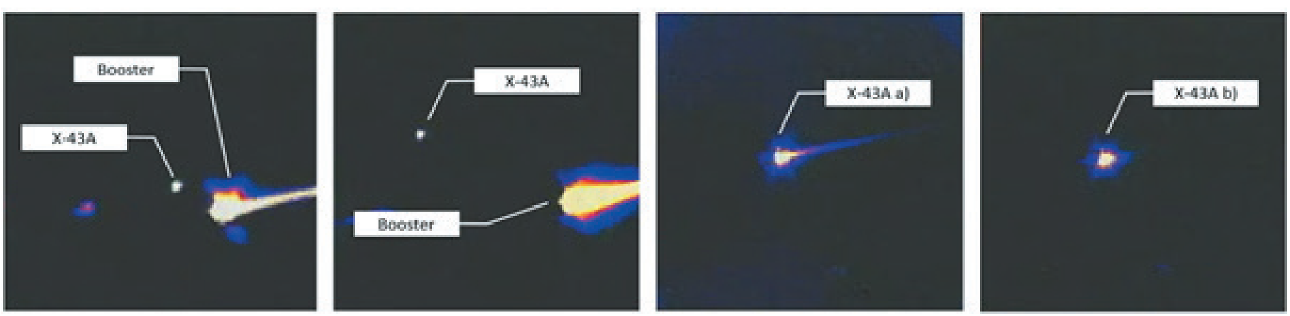

Figure 1. Separation and HALO-II experimental recording

cloud cover and haze. To reduce computational complexity, the scenario focused on aerial interactions without terrain modeling. Synthetic scenes were designed to include high-speed targets against varied spectral backgrounds, simulating EO/IR sensors of view at multiple altitudes and angles.

In Figure 2, we illustrate the simulation architecture developed using Ansys STK to model the flight and observation of the X-43A hypersonic aircraft during its unpowered flight phase.

The setup used a B-52 aircraft as the launch platform, with its flight path replicated from the actual experiment to accurately represent the mission's starting phase. The X-43A was designed with special attention to how separation occurred from the booster rocket, which marked the beginning of its sustained flight. The powered phase, including the sustain phase of the X-43A, was included from the scope of this analysis. The setup accounted for operational constraints by defining 20-35 km altitude ranges and velocity profiles from Mach 5 to Mach 10, reflecting real-world flight dynamics of hypersonic vehicles. The scenario depicted in Figure 3 included multiple observational platforms to monitor and analyze the unpowered flight: the HALO-II telemetry system with an EOIR camera platform and a satellite platform equipped with EOIR capabilities.

To replicate the experiment, the platforms were reconstructed, and a scenario was created in STK to simulate the unpowered flight phase in full detail.

3.3. SENSOR CONFIGURATIONS

Multiple EO/IR sensor configurations, HALO-II, Satellite, and Modified HALO-II, were tested, each parameterized with the spectral response, angular field of view, integration time, and resolution. Due to the unavailability of declassified data regarding the sensors, simulations were conducted to approximate and analyze the presented scenarios. A multi-sensor system was proposed, with sensors placed on simulated satellite and flight platforms. Each sensor was mounted on an independent gimbal, allowing it to collect different data points that gave a full picture of the target's radiometric signature. The Mod. HALO-II is a modified version of the previously analyzed HALO-II sensor, specifically designed and optimized to meet the requirements of ATR applications.

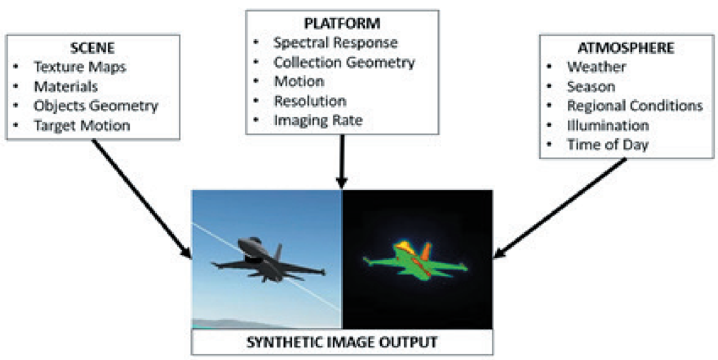

Figure 2. Ansys STK input components

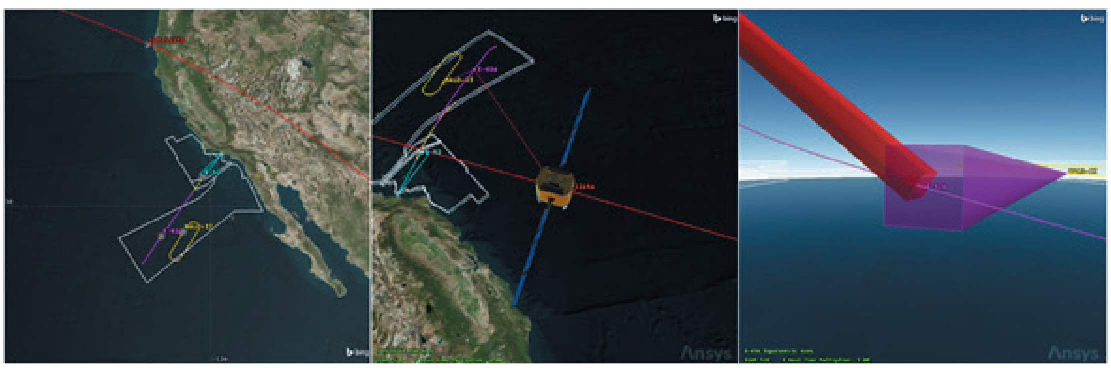

Figure 3. Modelled scenario with 2D planar view of the mission as well as 3D view and FOV of the EOIR sensors

Table 1 shows that both HALO-II and Satellite function within a similar spectral range, which makes them well-suited for mid-wave infrared applications, including thermal imaging and environmental monitoring. The modified HALO-II, featuring a wider spectral range, improves its capacity to capture a variety of thermal and material signatures, thus making it an ideal choice for applications that require broader spectral coverage.

Table 2 presents the FOV analysis, revealing key differences in the scheme of the sensors. The HALO-II system features a geometric FOV of 0.4°, which allows it to cover a broader scene while still offering enough precision for fine angular details. On the other hand, the modified HALO-II has a similar number of pixels but delivers a slightly smaller effective FOV, which can be observed as striking a balance between resolution and coverage. Satellite, optimized for fine-resolution tasks, has a much smaller geometric FOV and instantaneous FOV, prioritizing high angular precision over coverage.

4. RESULTS

The Modulation Transfer Function (MTF) characteristics reveal distinct different sensor behaviors across the spatial frequency spectrum, as shown in Table 3. HALO-II exhibits a relatively steep decline in MTF at higher spatial frequencies, indicating a reduction in resolution and contrast for smaller targets. The decline in optics MTF is sharper compared to jitter and detector footprint MTFs, suggesting optical limitations as a key factor in high-frequency degradation. Mod. HALO-II shows a smoother MTF decline across frequencies, maintaining higher resolution at mid-to-low frequencies and being suitable for detecting moderately sized targets. Conversely, the Satellite demonstrates consistent MTF performance across spatial frequencies, reflecting robust optical and detector design tailored for uniform imaging tasks.

Table 1. Spectral Band Comparison

Sensor	Low Band Edge Wavelength (μm)	High Band Edge Wavelength (μm)
Satellite	3.0	5.5
HALO-II	3.0	5.5
Mod. HALO-II	2.5	6.0

Table 2. Geometric and Effective FOV Comparison

Attribute	Satellite	HALO-II	Mod. HALO-II
Horizontal Pixels	640.0	640.0	640.0
Vertical Pixels	640.0	640.0	640.0
Geometric FOV	7.8e-08	4.87e-05	4.87e-05
Horizontal Geometric FOV (deg)	0.016	0.4	0.4
Vertical Geometric FOV (deg)	0.016	0.4	0.4
Geometric Instantaneous FOV (Sterad)	1.9e-13	1.19e-10	1.19e-10
Horizontal Geometric Instantaneous FOV (mrad)	0.000436	0.0109	0.0109
Vertical Geometric Instantaneous FOV (mrad)	0.000436	0.0109	0.0109
Effective FOV (Sterad)	1.55e-05	7.12e-05	6.33e-05
Horizontal Effective FOV (deg)	0.226	0.484	0.456
Vertical Effective FOV (deg)	0.226	0.484	0.456
Effective Instantaneous FOV (Sterad)	3.79e-11	1.74e-10	1.55e-10
Horizontal Effective Instantaneous FOV (mrad)	0.00616	0.0132	0.0124
Vertical Effective Instantaneous FOV (mrad)	0.00616	0.0132	0.0124

Table 3. MTF Trends

Sensor	Spatial Frequency (cycle/mrad)	MTF Trends
HALO-II	Range (0 to 454 mrad)	Steep decline at high frequencies; optical limitations evident
Satellite	Range (0 to 235 mrad)	Consistent MTF performance; robust optical and detector design
Mod. HALO-II	Range (0 to 200 mrad)	Smoother decline, retaining resolution at mid-to-low frequencies

Table 4. Optical Specification Comparison

Specification	Satellite	HALO-II	Mod. HALO-II
Effective Focal Length (cm)	415.0	415.0	100.0
F Number	4.15	2.15	2.0
Diffraction Wavelength (μm)	4.25	4.25	2.5
Airy Disk Diameter (mrad)	0.0104	0.00537	0.0122
Rayleigh Resolution (mrad)	0.00519	0.00269	0.0061
Sparrow Resolution (mrad)	0.00425	0.0022	0.005
Ensquared Energy	0.005	0.685	0.77

Table 5. Sensor Responsivity and Noise Comparison

Metric	Satellite	HALO-II	Mod. HALO-II
Peak Irradiance Responsivity (cm^2/W)	4.17e+19	2.12e+22	1.33e+21
Sensor NEI (W/cm^2)	1e-15	1e-15	1e-15
Sensor SEI (W/cm^2)	3e-12	3e-12	3e-12
Peak Radiance Responsivity ($cm^2 \cdot Sterad/W$)	1.56e+9	3.49e+12	1.94e+11
Sensor NER ($W \cdot cm^{-2} \cdot Sterad^{-1}$)	2.67e-05	6.06e-06	6.88e-06
Sensor SER ($W \cdot cm^{-2} \cdot Sterad^{-1}$)	0.0802	0.0182	0.0206

HALO-II features an effective focal length of 415 cm and a relatively small F-number, resulting in a smaller Airy disk diameter and finer Rayleigh resolution, as shown in Table 4. This enables high spatial resolution and angular precision. Mod. HALO-II, with a shorter focal length and a slightly larger F-number, achieves a coarser resolution but offers broader field coverage and enhanced ensquared energy. Satellite focuses on mid-wave infrared imaging with a narrower F-number and comparable diffraction-limited resolution to HALO-II but significantly lower ensquared energy, prioritizing light collection efficiency for stable environmental conditions.

HALO-II excels in responsivity metrics, shown in Table 5, demonstrating high sensitivity to weak signals and suitability for low-light imaging. Mod. HALO-II, even while having slightly lower responsivity than HALO-II, compensates with superior noise performance and signal stability, making it suitable for capturing thermal contrasts. Satellite delivers reliable performance in both responsivity and noise management, striking an optimal balance between sensitivity and robustness for steady-state imaging tasks.

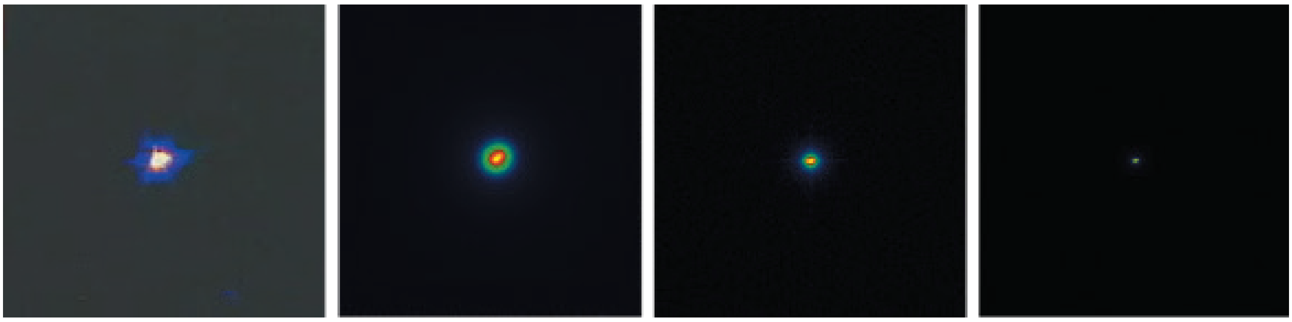

Figure 4. Comparison of experimental and synthetic data. The left panel shows the experimental data, followed by the Satellite data in the middle-left panel, HALO-II in the middle-right panel, and the Mod. HALO-II data on the far-right panel

Figure 5. ATR data set generated using Mod. HALO-II sensor model

This comparative analysis highlights the distinctive design philosophies of the three sensors depicted in Figure 4. Satellite demonstrates moderate performance across most metrics, optimized for mid-wave infrared applications requiring precise FOV control and high angular precision. HALO-II balances sensitivity, resolution, and coverage, making it suitable for versatile applications, particularly in low-light or broad-scene imaging. Mod. HALO-II excels in high-resolution imaging, superior angular precision, and broad spectral coverage, making it ideal for advanced ATR dataset generation and thermal imaging tasks.

The Mod. HALO-II sensor represents an optimized balance between resolution, field coverage, signal fidelity, and spectral versatility, making it a superior choice for ATR dataset generation, as depicted in Figure 5.

Building on the capabilities of the original HALO-II, Mod. HALO-II is designed to capture diverse, high-quality data, ensuring robust ATR model training and enabling algorithms to generalize effectively across multiple operational scenarios. With its ability to handle diverse targets and environments, Mod. HALO-II supports the creation of comprehensive ATR datasets. These datasets capture key target attributes, including high-speed motion smear, thermal signatures, and environmental effects under varying conditions, such as clear skies, degraded visual environments (e.g., haze and cloud cover), and changes in the angular field of view and spectral response.

5. CONCLUSION

The use of synthetic datasets generated with ANSYS STK tools has proven to be an effective approach for modeling hypersonic vehicle detection scenarios, and ATR dataset generation, addressing significant data gaps in this field. These simulations have provided valuable insights into the operational behavior of EOIR sensors while also demonstrating an efficient workflow for ATR dataset creation. This methodology not only supports current research efforts but also establishes a reliable framework for future advancements in hypersonic detection and analysis. Future research should focus on the synergistic integration of synthetic datasets with experimental data to improve the adaptability and generalization capabilities of algorithms. By refining these methodologies, we can significantly enhance detection capabilities, paving the way for the seamless integration of synthetic data into AI-driven detection systems addressing the challenges posed by emerging hypersonic threats.

REFERENCES

[1] C. R. McClinton, L. T. Nguyen, J. R. Sitz and L. V. Rausch, "Preliminary X-43 flight test results," *Acta Astronautica*, 2005.

[2] P. T. Harsha, L. C. Keel, A. Castrogiovanni and R. T. Sherrill, "X-43A Vehicle Design and Manufacture," *AIAA/CIRA 13th International Space Planes and Hypersonics Systems and Technologies*, 2005.

[3] C. McClinton, "X-43: Scramjet Power Breaks the Hypersonic Barrier," *NASA, Dryden Lecture*, 2006.

[4] R. R. Kazmar, "Airbreathing Hypersonic Propulsion at Pratt & Whitney – Overview," *AIAA*, 2005.

[5] S. Hinterstoisser, V. Lepetit, P. Wohlhart and K. Konolige, "On Pre-Trained Image Features and Synthetic Images for Deep Learning," *Computer Vision – ECCV 2018 Workshops*, p. pp 682–697, 2018.

[6] S. Webster, M. Jeiran, K. Manser, N. Pinto and S. Harkrider, "Synthetic Imagery Generation," *NATO-OTAN, S&T Organization*, 2006.

[7] J. Tremblay, A. Prakash, D. Acuna, M. Brophy, V. Jampani, C. Anil, T. To, E. Cameracci, S. Boochoon and S. Birchfield, "Training Deep Networks with Synthetic Data: Bridging the Reality Gap by Domain Randomization," *IEEE/CVF Conference on Computer Vision and Pattern Recognition Workshops*, 2018.

[8] A. Handa, V. Patraucean,.V. Badrinarayanan,. S. Stent and R. Cipolla, "Understanding Real World Indoor Scenes With Synthetic Data," *IEEE Conference on Computer Vision and Pattern Recognition (CVPR)*, 2016.

[9] G. Ros, L. Sellart, J. Materzynska, D. Vazquez and A. M. Lopez, "The SYNTHIA Dataset: A Large Collection of Synthetic Images for Semantic Segmentation of Urban Scenes," *IEEE Conference on Computer Vision and Pattern Recognition*, 2016.

[10] S. Han, A. Farfard, J. P. Kerekes, M. G. Gartley, E. J. Ientilucci, A. Savakis, C. Law, J. Parhan, M. Turek, K. Fieldhouse and T. Rovito, "Efficient generation of image chips for training deep learning networks," *Proceedings of SPIE - The International Society for Optical Engineering*, 2017.

[11] J. Graybeal, J. Quartuccio and T. Du Bosq, "Immersive Simulation, Prototyping, and Evaluation of Infrared Sensor and Augmented Reality Technologies," *NATO-OTAN, S&T Organisation*, 2012.